Journal of Physiology (1993), **472**, *pp.* 127–156
With 13 *figures*
Printed in Great Britain

BIREFRINGENCE CHANGES ASSOCIATED WITH ISOMETRIC CONTRACTION AND RAPID SHORTENING STEPS IN FROG SKELETAL MUSCLE FIBRES

BY MALCOLM IRVING

From the Molecular Biology and Biophysics Section, Division of Biomedical Sciences, King's College London, 26–29 Drury Lane, London WC2 5RL

(*Received 25 August 1992*)

SUMMARY

1. Muscle birefringence, the difference between the refractive indices of light polarized parallel and perpendicular to the muscle fibre axis, was measured at 3 °C in intact single fibres isolated from frog muscle. Resting birefringence was $2{\cdot}20 \pm 0{\cdot}02 \times 10^{-3}$ (mean ± S.E.M., $n = 44$) at sarcomere length 2·4–2·7 μm and $2{\cdot}35 \pm 0{\cdot}03 \times 10^{-3}$ ($n = 19$) at 3·5–3·8 μm.

2. Birefringence decreased during isometric twitch or tetanic contractions. The peak change in a twitch at sarcomere length 2·6 μm, determined by two independent methods, was $0{\cdot}150 \pm 0{\cdot}017 \times 10^{-3}$ (mean ± S.E.M., $n = 6$). The corresponding value after 0·4 s of tetanic stimulation was $0{\cdot}167 \pm 0{\cdot}012 \times 10^{-3}$ ($n = 6$).

3. The birefringence change had a shorter latency than tension and reached its half-maximum value earlier than tension. The difference in time to half-maximum in tetani was 11·5 ± 1·3 ms (mean ± S.E.M., $n = 6$) at 3 °C. After stimulation birefringence recovered to its pre-stimulus baseline more slowly than tension.

4. The birefringence decrease after 0·4 s of tetanic stimulation was linearly related to the expected degree of overlap between actin and myosin filaments in the sarcomere length range 2·6–3·6 μm. The amplitude of the birefringence decrease at full filament overlap (sarcomere length 2·2 μm) was estimated to be $0{\cdot}235 \pm 0{\cdot}015 \times 10^{-3}$.

5. Birefringence changes associated with shortening steps of 0·9% fibre length at sarcomere length 2·6 μm exhibited four phases corresponding to those of the tension transient. There was no consistent birefringence change during the length step itself. During the rapid tension recovery birefringence increased by $0{\cdot}014 \pm 0{\cdot}001 \times 10^{-3}$ ($n = 3$), measured from the end of the length step to 2 ms later. Birefringence continued to increase as tension recovery slowed, reaching a peak about 10 ms after the step, then recovered with a rate similar to that of the final tension recovery.

6. These birefringence changes are likely to be caused by axial rotation of the head domain of the myosin cross-bridge. During isometric contraction heads bind to actin with their long axes more perpendicular to the fibre axis than in resting muscle, although there is likely to be a wide range of head orientations during contraction. The small birefringence increase during the rapid tension recovery following a

shortening step is consistent with myosin head rotation during the elementary force-generating process in the attached myosin–actin complex.

INTRODUCTION

The generation of force and shortening by muscle is not yet understood at the molecular level. Relative sliding between actin and myosin filaments is generally considered to be produced by a 'working stroke' in the myosin cross-bridge or head domain while it is attached to actin. The working stroke is expected to produce an axial displacement of the actin-attached end of the myosin head by about 10 nm with respect to its origin on the myosin filament (A. F. Huxley & Simmons, 1971; Irving, Lombardi, Piazzesi & Ferenczi, 1992), so an axial rotation of the head may be involved, but there is so far no clear evidence for this hypothesis (Cooke, 1986; Irving, 1987). It is difficult to investigate the working stroke by structural methods, because it normally occurs asynchronously in the population of myosin molecules and, even when partially synchronized by a rapid perturbation of muscle length, is complete within a few milliseconds (A. F. Huxley & Simmons, 1971). The use of such length perturbations combined with fast time-resolved structural measurements seems a promising approach to investigate the structural basis of the working stroke. The present experiments combine this approach with measurements of muscle birefringence to follow changes in the orientation of the myosin heads.

The use of birefringence to study muscle contraction has a long history, and the early work has been reviewed by Høncke (1947) and A. F. Huxley (1977). Muscle has a higher refractive index for light which is polarized along the fibre axis than for that polarized perpendicular to it, i.e. it is birefringent. In striated muscle nearly all the birefringence is associated with the myosin-containing anisotropic (A) bands of the sarcomere, suggesting that it is due to the alignment of the myosin filaments with the fibre axis. About 60 % of the total birefringence – the form birefringence – is due to the higher refractive index of the oriented proteins compared to that of cytoplasm (Noll & Weber, 1934; Obiorah & Irving, 1989). The remainder – the intrinsic birefringence – is due to the polarization dependence of the refractive index of the proteins themselves. Both types of birefringence depend on the degree of alignment of the oriented proteins with the fibre axis.

Muscle birefringence decreases during contraction (von Muralt, 1932; Bozler & Cottrell, 1937; Eberstein & Rosenfalck, 1963). The amplitude of the decrease is roughly proportional to the expected degree of overlap between actin and myosin filaments (Eberstein & Rosenfalck, 1963), i.e. to the fraction of myosin cross-bridges that can interact with actin. A birefringence decrease with similar amplitude and sarcomere length dependence occurs when relaxed demembranated fibres are put into rigor (Taylor, 1976; Peckham & Irving, 1989). The sarcomere length dependence of these birefringence changes suggests that they are caused by changes in the orientation of the myosin cross-bridges as they bind to actin in active contraction or in rigor. A quantitative theory relating muscle birefringence to the orientation of the component domains of myosin has been developed, and shows that the observed birefringence changes are consistent with plausible changes in the orientation of the myosin head domain (Irving, Peckham & Ferenczi, 1988; Haskell, Carlson & Blank, 1989; Peckham & Irving, 1989). Birefringence measurements can therefore be used

to follow changes in the orientation of the myosin head domain in contracting muscle fibres.

METHODS

Fibre preparation and mounting

Frogs (*Rana temporaria*) were killed by decapitation followed by destruction of the spinal cord. Single fibres were dissected from the dorsal head of the anterior tibialis muscle using sharpened stainless-steel needles to cut fine strands of connective tissue between the fibres. The dissecting dish was cooled to 5 °C. Fibres were selected for large diameter, flattened cross-section, low opacity and strong tendon attachments. Any opaque or birefringent material loosely adhering to the fibre was removed. Tendons were thoroughly cleaned of debris from other fibres and cut to fit aluminium T-clips of the type described by Ford, Huxley & Simmons (1977). The tendon tabs were clamped between the arms of the T about 50 μm from the end-most striations of the fibre. The dissection and experiments were carried out in Ringer solution containing (mM): NaCl, 120; KCl, 2·5; $CaCl_2$, 1·8; Na_2HPO_4, 2·15; NaH_2PO_4, 0·85; pH 7·1 at 0 °C.

Immediately after dissection, fibres were transferred to the experimental chamber, which was mounted on the stage of a polarizing microscope. The T-clips were hung on co-axial hooks made from electrolytically sharpened stainless-steel wire, 150 μm in diameter. The hooks used in most experiments (Figs 2–7) could be rotated about the fibre axis in sleeves made from hypodermic needle tubing. For experiments involving rapid changes of fibre length these were replaced by lighter fixed hooks. One of the hooks was always attached to a motor for controlling fibre length and the other to a force transducer (see below). The temperature of the fibre and bathing solution was held at 2–4 °C using Peltier cooling units under feedback control from a thermocouple in the experimental chamber. Fibres were stimulated by 0·1 ms pulses of transverse current, about 1·5 times threshold intensity, via a pair of blackened platinum electrodes, 12 × 3 mm, about 6 mm apart and adjusted to be parallel to the fibre axis. Fused tetani were elicited by stimulation at 15–25 Hz.

Mechanical measurements

The force transducer used in most of the experiments (SensoNor AE801, Horten, Norway) was critically damped. The resonant frequency of the transducer and hook assembly was 2·0 kHz with the rotating hook and 6·2 kHz with the fixed hook. The motor system was as described by Ford *et al.* (1977) and could produce movements of 1 % fibre length which were complete in 0·2 ms. The force transducer and motor hooks were adjusted to be precisely co-axial and passed into the experimental chamber through vertical slots in its ends. In two experiments (Fig. 10) the average sarcomere length in 1–2 mm segments of a fibre was measured with a striation follower (A. F. Huxley, Lombardi & Peachey, 1981). These experiments used a capacitance gauge force transducer (A. F. Huxley & Lombardi, 1980) and a loudspeaker motor (Cecchi, Colomo & Lombardi, 1976).

Optical measurements

The experimental chamber was mounted on the rotating stage of a modified polarizing microscope with the fibre horizontal. The optical components are shown schematically in Fig. 1. The light source was a He–Ne laser, beam diameter about 2 mm. A telescope with cylindrical lenses CL1 and CL2 expanded the beam diameter by about 10 times in the direction of the fibre axis. For wide-field illumination an adjustable slit, S, was imaged at the fibre plane, with a magnification of about 0·3, by spherical lens SL1. A thin glass coverslip formed the base of the experimental chamber. The image of the slit was adjusted to be about 0·7 mm long and in the first series of experiments was 30–60 % wider than the fibre (wide-field illumination, Figs 2–7) except where stated. In the second series, fibres were compressed between glass coverslips (Figs 8 and 9) and the width of the slit was adjusted to be about half the fibre width, so that a region of uniform optical path length was illuminated. The intensity of the illuminating light beam (I_i) was monitored by a photodiode, PD3. In a few experiments the variation of optical properties across the fibre width was studied by removing lenses CL1, CL2 and SL1, and slit S, and using a single spherical lens, $f = 25$ mm, to focus the beam to an approximately 20 μm diameter spot at the fibre.

The principle of the birefringence measurements is described in the Appendix (Fig. 11). The illuminating light was polarized at 45 deg to the fibre axis by a dichroic sheet polarizer (POL; Figs 1 and 11). After the polarizer the light can be considered as being composed of 0 deg and 90 deg

components (relative to the fibre axis) of equal intensity and phase. A Babinet–Soleil compensator (BS) (Halle, Berlin) with its slow (i.e. higher refractive index) axis at 90 deg was used to introduce a calibrated retardation (θ) between these two components. The muscle fibre (MF) also introduces a retardation (ϕ), of the opposite sign to that introduced by the compensator, as a result of its

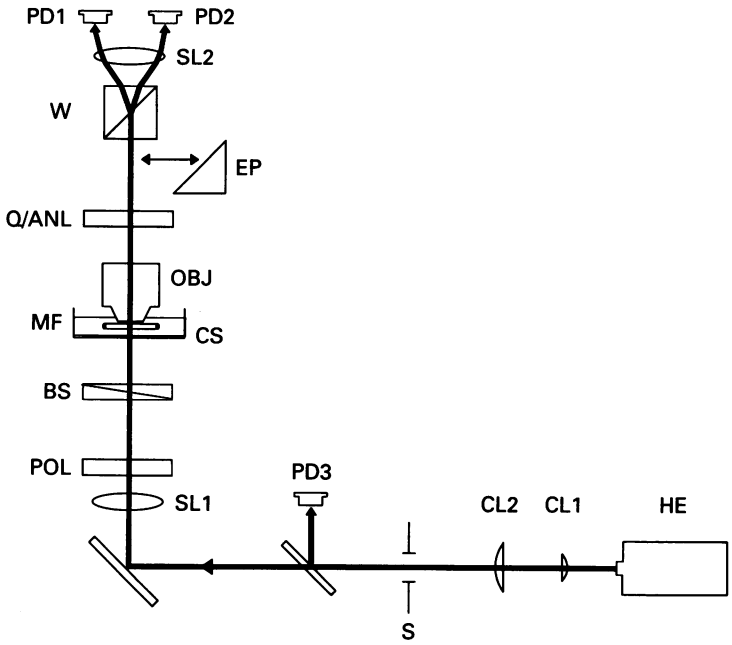

Fig. 1. Schematic diagram of the optical apparatus used to measure muscle fibre retardation. HE, 5 mW He–Ne laser. CL1 and CL2, cylindrical lenses. S, adjustable field slit. SL1, spherical lens forming an image of S at the muscle fibre. POL, dichroic sheet polarizer. BS, Babinet-Soleil compensator (Halle, Berlin). CS, glass coverslip. MF, muscle fibre. OBJ, water immersion objective (Nikon 10×, NA 0·22). Q, quarter-wave plate. ANL, analyser. EP, eyepiece prism. W, Wollaston prism. SL2, spherical lens forming images of the back focal plane of OBJ on two photodiodes PD1 and PD2 (Mullard BPX42). PD3, similar photodiode monitoring the intensity of the illuminating light beam.

birefringence. For steady-state measurements of fibre retardation the light collected by the objective (OBJ) was viewed through an analyser (ANL) with its transmission axis perpendicular to that of the polarizer (Fig. 11), using eyepiece prism EP (Fig. 1). With wide-field illumination, and the compensator retardation θ set to zero, fibres appear bright against a black background. As θ is increased two dark bands move in from the edges of the fibre towards the centre (shown in Plate 1 of Baylor & Oetliker, 1977). When the dark bands fuse, giving the darkest field at the thickest part of the fibre cross-section, the compensator retardation is equal to the fibre retardation at this point (Appendix, eqn (A5)). In some experiments this null retardation was obtained by illuminating the fibre with a 20 μm diameter spot of light (see above) at the thickest part of the cross-section; this gave more reproducible retardation values. All fibre retardation measurements were corrected for the small background birefringence of the set-up by subtracting the corresponding values obtained with the fibre moved out of the illuminating beam. The optical path length at the thickest point of the fibre cross-section was assumed to be equal to the fibre width measured after the fibre had been rotated by 90 deg about its axis.

For continuous retardation measurements the eyepiece prism was removed and the analyser was replaced by a quarter-wave plate (Q) with its slow axis parallel to the polarizer axis. The light was

then split into 0 deg and 90 deg components by a Wollaston prism (W) and the intensities of these two components, I_0 and I_{90} respectively, measured by photodiodes PD1 and PD2 (Mullard BPX42, Siemens, Germany) (Figs 1 and 11). The ratio $R = (I_0 - I_{90})/(I_0 + I_{90})$ is equal to the sine of the net retardation, i.e. $\sin(\phi - \theta)$ (eqn (A10)). R was calculated electronically from the amplified outputs of PD1 and PD2 and filtered with a two-pole 10 kHz Bessel filter. Similarly a signal proportional to $(I_0 + I_{90})/I_i$ was calculated electronically from the amplified outputs of PD1, PD2 and PD3. $(I_0 + I_{90})/I_i$ is proportional to the fraction of the incident light transmitted by the fibre and slit and collected by the objective (Appendix, eqn (A16)). Tension, motor position, R and $(I_0 + I_{90})/I_i$ signals were digitized for storage and analysis, with a sample interval of 1 or 2 ms during the rising phase of a twitch or tetanus and 10 or 20 ms thereafter. The signals associated with rapid shortening steps were recorded with a 20 μs sample interval using a Datalab transient recorder.

Preliminary measurements showed that serious movement artifacts could be produced by changes in cross-sectional shape of the fibres on stimulation. These were reduced by stretching the fibres to a sarcomere length of at least 2·6 μm (measured with a 40 ×, 0·65 numerical aperture (NA) objective) before stimulation, and by appropriate selection and mounting of the fibres, as described above. In the first series of experiments (wide-field illumination, Figs 2–7) the rotating hooks were set to remove twist in the fibre, and the major axis of the fibre cross-section was initially set horizontal. Fibres which twisted or exhibited large longitudinal or transverse movements on stimulation at sarcomere length 2·6 μm were rejected. In accepted fibres a region that was free of adhering birefringent material and in which changes of width and depth on stimulation could not be detected by eye was selected for optical recording. The retardation at the thickest part of the fibre cross-section was determined visually by the null method described above. Resting fibre transmittance was determined from the ratio of values of $(I_0 + I_{90})/I_i$ with the fibre in and out of the illuminated region (eqn (A16)). Linear dichroism of the resting fibre was measured by removing the quarter-wave plate (eqn (A9)). Fibre and slit width were measured by photographing the fibre through the 10 × objective and an 8 × eyepiece, using 1/1000 s exposure on Ilford XP1 film. Sarcomere length was also measured from the photographs. The fibre was then rotated through 90 deg about its axis and photographed again in order to determine the orthogonal dimension. Before stimulation the compensator was set to give $R = 0$ for the whole illuminated region (the fibre plus the light bypassing it in the slit). Fibres were photographed during two contractions, before and after 90 deg rotation. Retardation transients associated with a contraction were recorded, then a second set of 0 deg and 90 deg photographs was obtained at rest and during contraction. Fibres were included in the analysis if both cross-sectional dimensions changed by less than 3% on stimulation (see Appendix).

In the second set of experiments (Figs 8 and 9) fibres were lightly compressed between two strips of glass coverslip, about 3 mm wide, each bent into a flat-bottomed U-shape so that the centres of the U's formed horizontal planes in contact with the top and bottom surfaces of about 3 mm length of fibre. The coverslips were coated with dichlorodimethylsilane to reduce friction at the contact with the fibre surface. The lower (inverted) U was fixed to the base of the experimental chamber so that a fibre mounted on the hooks rested on the horizontal coated surface. The upper U was mounted on the microscope objective used for the optical measurements with the horizontal surface in the focal plane; the degree of fibre compression was controlled with the fine focus adjustment. Retardation measurements on compressed fibres were made as described above. The optical path length in the fibre was not measured, but was assumed to remain constant on stimulation.

RESULTS

Birefringence of resting fibres

Fibre birefringence was determined from optical retardation divided by optical path length (eqn (A1)). The fibre retardation was obtained from the compensator retardation which gave the darkest appearance of the thickest part of the fibre cross-section when it was viewed between crossed polarizers (see Methods and Appendix, eqns (A1)–(A5)). The observed fibre retardation was approximately linearly related to fibre diameter, or optical path length (Fig. 2), and resting birefringence was determined by linear regression on these data (eqn (A1)).

In the sarcomere length range 2·4–2·7 μm (Fig. 2, circles) the resting birefringence was $2{\cdot}20 \pm 0{\cdot}02 \times 10^{-3}$ (mean ± S.E.M., $n = 44$; continuous regression line). In the sarcomere length range 3·5–3·8 μm (triangles) the resting birefringence was $2{\cdot}35 \pm 0{\cdot}03 \times 10^{-3}$ ($n = 19$; dashed regression line). In six fibres the paired difference

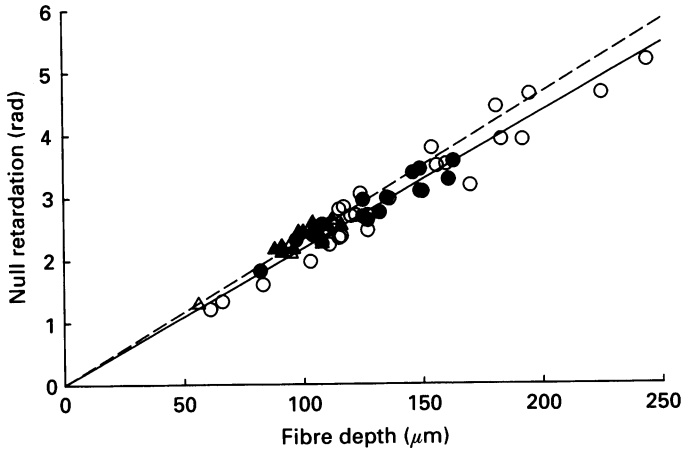

Fig. 2. Optical retardation of resting fibres plotted against fibre depth or optical path length. Retardation was determined by a null method using a Babinet–Soleil compensator, as described in Methods. Circles: sarcomere length 2·4–2·7 μm, forty-four observations on thirteen fibres; triangles: sarcomere length 3·5–3·8 μm, nineteen observations on six fibres. The data in each sarcomere length range were least-squares fitted to a straight line constrained to pass through the origin. The gradients were $0{\cdot}0218 \pm 0{\cdot}0002$ rad/μm (sarcomere length 2·4–2·7 μm; continuous line) and $0{\cdot}0233 \pm 0{\cdot}0003$ rad/μm (sarcomere length 3·5–3·8 μm; dashed line). The fibre birefringence can be obtained from these gradients by multiplying by $\lambda/2\pi$ (Appendix, eqn (1); $\lambda = 0{\cdot}633$ μm). Open symbols represent data obtained using wide-field illumination; closed symbols those obtained by illumination with a 20 μm diameter spot. There was no significant difference between the gradients of regression relations obtained by the two methods at either sarcomere length.

between resting birefringence values in these two sarcomere length ranges (long–short) was $0{\cdot}22 \pm 0{\cdot}04 \times 10^{-3}$, which is significant at the 0·5% level (t test). However, the difference is small and may be due to the systematic change in fibre cross-section with sarcomere length (Blinks, 1965). At the shorter sarcomere length, the ratio of major to minor axes of fibre cross-section (considered as an ellipse) was 1·1–2·7 (mean 1·62) for the fibres in Fig. 2; at the longer sarcomere length it was 1·00–1·06 (mean 1·03). At the shorter sarcomere length irregularities of fibre shape might have led to a slight overestimate of optical path length (determined by rotating the fibre by 90 deg and measuring its width) and thus an underestimate of the birefringence. This is unlikely to have happened at the long sarcomere length, at which fibres have a roughly circular cross-section.

The method of measuring birefringence that was used for the data shown in Fig. 2 is too slow to be useful for time-resolved measurements on contracting muscle fibres. For this purpose a continuous optoelectronic method of determining fibre retardation was used (eqns (A6)–(A17)). In this method the analyser (Figs 1 and 11)

was replaced by a quarter-wave plate which converts the phase difference between the light components parallel and perpendicular to the fibre axis (the fibre retardation, ϕ) into an intensity difference between these two components. These were then separated by a polarizing beam-splitting prism and the intensities (I_0 and I_{90}) measured with photodiodes. When a small uniform region of a muscle fibre is illuminated, the ratio R of the difference to the sum of the intensities measured by the photodiodes is simply given by:

$$R = (I_0 - I_{90})/(I_0 + I_{90}) = \sin(\phi - \theta),$$

where θ is the retardation introduced by the compensator (eqn (A10)).

In the first series of experiments (Figs 3–7) the illuminating light beam was made wider than the fibre to minimize artifacts due to fibre movement. In this case, if the fibre cross-section is assumed to be elliptical, R is given by eqn (A15):

$$R = (1-g)S - g\sin\theta,$$

where

$$S = \tfrac{1}{2}\pi J_1(\phi_c)\cos\theta - [1 - \tfrac{1}{2}\pi H_1(\phi_c)]\sin\theta,$$

and J_1 and H_1 are, respectively, Bessel and Struve functions of first order, ϕ_c is the retardation for the ray passing through the thickest part of the fibre cross-section and g is the effective fraction of light passing the fibre, taking into account fibre scattering and absorbance; g is given by $f/[(1-f)T+f]$, where f is the actual fraction of the illuminating light which bypasses the fibre and T is the fibre transmittance, defined as the fraction of the light incident on the fibre which is transmitted by it and collected by the objective (eqn (A16)).

These equations assume that, for a given fibre, T is independent of the part of the fibre cross-section traversed by the light beam, i.e. T has the same value for a ray passing through the centre of the fibre as for a ray traversing a smaller path length in the fibre near the edge. This assumption was tested by measuring transmittance with a 20 μm diameter spot of light. When the spot was positioned at the thickest part of the fibre cross-section T was $0{\cdot}809 \pm 0{\cdot}018$ (mean $\pm$ S.E.M., five fibres); when the spot was moved close to the edge of the fibre, where the optical path length (estimated from the retardation) was $0{\cdot}578 \pm 0{\cdot}029$ of that at the thickest part, T was $0{\cdot}844 \pm 0{\cdot}021$. In paired comparisons, T(edge)/T(thickest part) was $1{\cdot}043 \pm 0{\cdot}025$. Intermediate spot positions also gave ratios that were not significantly different from unity. Thus fibre transmittance appears to be roughly independent of the thickness of the part of the fibre traversed by the light beam. This may be due to the approximate cancellation, with the present optical set-up, of the greater light loss by absorbance and scattering near the centre of the fibre and the greater loss by refraction at the edges. Fibre transmittance was also approximately independent of the polarization of the incident light. In fifteen observations with wide-field illumination on ten fibres $T_0 - T_{90}$ was $0{\cdot}021 \pm 0{\cdot}013$ (mean $\pm$ S.E.M.) and $\frac{1}{2}(T_0 + T_{90})$ was $0{\cdot}758 \pm 0{\cdot}038$. Thus with the optical set-up used here resting fibre dichroism is small and not significantly different from zero.

Experimental values of the intensity ratio R for a fibre of typical dimensions are plotted in Fig. 3*A* (circles) as a function of the compensator retardation, θ. The continuous line shows values of R calculated from eqns (A14) and (A15), using the

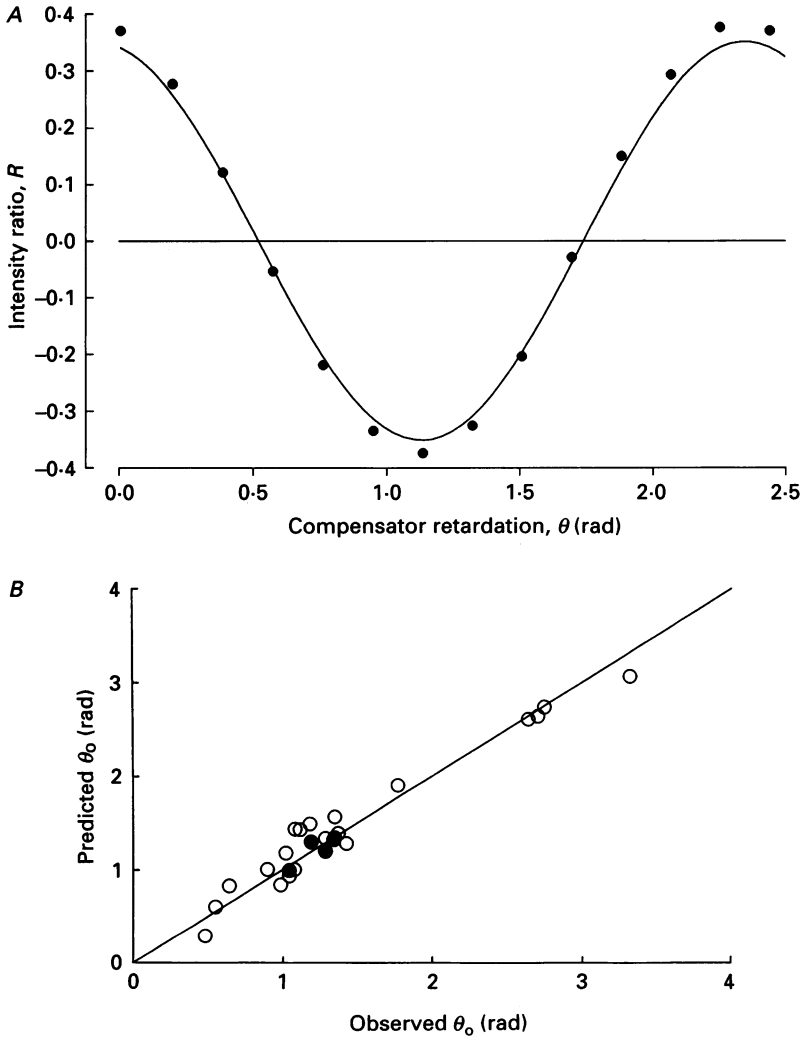

Fig. 3. Retardation measurements with wide-field illumination. *A*, comparison of measured intensity ratio $R = (I_0 - I_{90})/(I_0 + I_{90})$ (●) with the predicted value of R from eqns (A14) and (A15) (continuous line), as a function of compensator retardation, θ. Peak fibre retardation at thickest part of fibre cross-section (ϕ_c), determined by illuminating with a 20 μm diameter spot, 2·91 rad; fraction of illuminating light bypassing fibre (f), 0·332; fibre transmittance (T), 0·706; sarcomere length, 2·5 μm. *B*, comparison of observed and predicted values of the compensator retardation, θ_0, required to give $R = 0$. Predicted values are shown in the range $0 < \theta_0 < \pi$. Range of values of ϕ_c, 1·22–5·18 rad; range of values of f, 0·00–0·486; range of values of T, 0·516–0·954; sarcomere length, 2·5–2·8 μm; twenty-five observations on twelve muscle fibres. ○, ϕ_c determined using wide-field illumination; ●, ϕ_c determined using 20 μm spot illumination. The continuous line represents $y = x$.

measured values of f and T and the peak fibre retardation, ϕ_c, determined by viewing the fibre between crossed polarizers. There is reasonable but not exact agreement between the measured and calculated values of R as θ is varied.

The agreement between measured and calculated values of R was assessed in twelve fibres by comparing the measured values of the compensator retardation, θ_0, that gave $R = 0$ with the values predicted from eqns (A14) and (A15) and the measured values of ϕ_c, f and T (Fig. 3*B*, circles). Although there is some scatter about

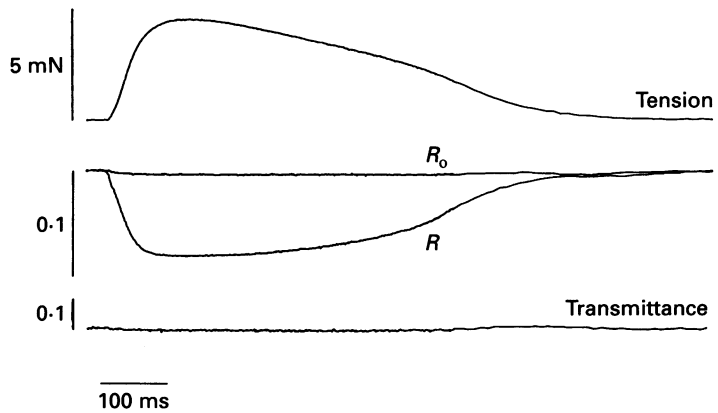

Fig. 4. Change in retardation associated with an isometric twitch. Traces from top to bottom show changes in tension, intensity ratio R_0 recorded in the absence of the quarter-wave plate (Figs 1 and 11), intensity ratio R recorded with the quarter-wave plate present, and total apparent transmittance $(I_0+I_{90})/I_i$. The baselines for tension and transmittance are at the bottom of the respective calibration bars; those for R and R_0 are at the top. Compensator retardation (θ), 1·37 rad; slit width, 317 μm; fibre length, 6·7 mm; temperature, 3 °C. Sample interval, 1 ms for the first 550 ms and 10 ms thereafter. The start of the time calibration bar marks the stimulus. Before stimulation fibre width was 244 μm; depth, 111 μm; sarcomere length, 2·57 μm; peak retardation at the thickest part of the fibre cross-section (ϕ_c), 2·22 rad; $(I_0+I_{90})/I_i$, 0·893. At 150 ms after the stimulus (shortly after the peak of the twitch) width was 246 μm; depth, 112 μm; sarcomere length, 2·55 μm.

the line of equality (continuous line), there is no systematic difference between measured and predicted values. The difference did not correlate strongly with fibre diameter, transmittance or slit width; it is likely to be due to the non-elliptical cross-section of the fibres (see Appendix).

Isometric twitch

A large decrease in fibre retardation accompanies an isometric twitch at sarcomere length 2·6 μm. Figure 4 shows changes in tension (upper), the intensity ratio R (centre) and total transmittance $(I_0+I_{90})/I_i$(lower) following single action potential stimulation at 3 °C. The trace labelled R_0 was obtained without the quarter-wave plate (Figs 1 and 11) and gives a measure of fibre dichroism (the difference in transmittance for light polarized at 0 deg and 90 deg to the fibre axis, T_0-T_{90}; eqn (A17)). Changes in dichroism associated with stimulation were small. (T_0-T_{90}) changed by typically 0·01, which is similar to the resting dichroism. In both cases negligible error is introduced into retardation measurements by fibre dichroism (see Appendix).

Changes in total transmittance, $(I_0+I_{90})/I_i$, and fibre transmittance T associated with stimulation were also of the order of 0·01 or less. The polarity and time course

of changes in total and dichroic transmittance varied from fibre to fibre. These signals may contain contributions from changes in fibre absorbance, scattering, diffraction or movement, and were not investigated further. Their amplitudes are too small to affect the accuracy of retardation measurements (see Appendix, Fig. 13).

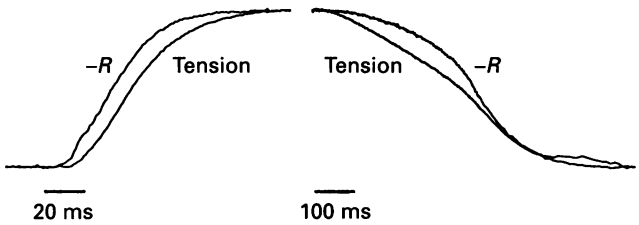

Fig. 5. Comparison of time courses of tension and intensity ratio R in an isometric twitch. From the same traces as Fig. 4, but the R trace has been inverted and scaled to the same peak as tension to facilitate time course comparison. Note that the time scale changes at the break in the traces at the peak. Stimulus is at the start of the left time calibration bar. Temperature, 3 °C.

The decrease in R seen with the quarter-wave plate in position (Fig. 4, centre) is due to a decrease in fibre birefringence. Photomicrographs of the fibre along two perpendicular axes showed that its major and minor diameters of cross-section changed from 244 and 111 μm in the resting fibre to 246 and 112 μm respectively at the peak of the twitch. From the measured changes in R and fibre transmittance (Fig. 4) and these dimensions, eqns (A14) and (A15) show that the peak decrease in fibre retardation was 0·184 rad. The decrease in birefringence was $0{\cdot}184 \times 10^{-3}$. The mean decrease in three well-immobilized fibres was $0{\cdot}160 \pm 0{\cdot}017 \times 10^{-3}$, which represents a decrease of about 7% of the resting birefringence.

The cross-sectional area of the fibres, estimated from the apparent diameters along two perpendicular axes, increased slightly during contraction, by $1{\cdot}84 \pm 0{\cdot}21$% (mean ± S.E.M.). The mean sarcomere shortening was $0{\cdot}90 \pm 0{\cdot}20$%, giving a net increase in sarcomere volume of $0{\cdot}85 \pm 0{\cdot}17$%. This volume change is too small to be responsible for the observed birefringence decrease (see Discussion).

The time course of the change in R was similar but not identical to that of tension development. In Fig. 5 the R signal has been inverted and scaled to the same peak amplitude as tension. In the conditions of Figs 4 and 5 changes in optical path length and fibre transmittance were negligible, so the change in R is expected to be directly proportional to that in birefringence, and therefore to have the same time course (Appendix, Fig. 13). Birefringence has a shorter latency than tension; this is expected because of the small early components of the birefringence change which have time courses similar to those of the muscle action potential and the intracellular calcium transient (Baylor & Oetliker, 1977; Baylor, Chandler & Marshall, 1984). These components are also seen at sarcomere lengths great enough to largely eliminate overlap between actin- and myosin-containing filaments (ibid.).

The temporal lead of birefringence over tension is maintained throughout the rising phase of the twitch. The time from the stimulus to half-maximum birefringence in twitches at 3 °C was $36{\cdot}4 \pm 1{\cdot}3$ ms (mean ± S.E.M., $n = 3$) and that to half-maximum tension was $45{\cdot}2 \pm 0{\cdot}6$ ms (paired difference $8{\cdot}8 \pm 1{\cdot}0$ ms). The temporal

lead of birefringence over tension is too large to be due to the presence of the early birefringence components described by Baylor & Oetliker (1977), which have a maximum amplitude of only about $0{\cdot}003 \times 10^{-3}$, compared with the peak change of $0{\cdot}160 \times 10^{-3}$ in a twitch at sarcomere length 2·6 μm.

In the falling phase of the twitch birefringence recovery lags tension relaxation (Fig. 5). This lag was consistently seen in the early 'isometric' part of the relaxation. However, the R traces sometimes (e.g. Fig. 6 below) showed large movement artifacts during the later phase of relaxation, presumably related to the large longitudinal movement of the fibres at this time.

Isometric tetanus

The magnitude of the birefringence decrease associated with tetanic stimulation (Fig. 6) at 3 °C is similar to that associated with a twitch. Changes in total and dichroic transmittance were again about 0·01 or less, introducing negligible error into the retardation measurements. The birefringence decrease estimated by the method used in the previous section was $0{\cdot}156 \pm 0{\cdot}018 \times 10^{-3}$ (mean ± S.E.M., $n = 3$) at 0·4 s in tetani at sarcomere length 2·6 μm. The cross-sectional area of the fibres estimated from the apparent diameters increased by $1{\cdot}19 \pm 0{\cdot}26$% during contraction. The mean sarcomere shortening was $0{\cdot}99 \pm 0{\cdot}35$%, giving an insignificant net increase in sarcomere volume of $0{\cdot}19 \pm 0{\cdot}50$%. During the rising phase of the tetanus the retardation change was faster than the tension increase; times to half-maximum at 3 °C were $40{\cdot}6 \pm 3{\cdot}3$ ms ($n = 3$) and $52{\cdot}3 \pm 5{\cdot}2$ ms respectively. The paired difference, $11{\cdot}7 \pm 2{\cdot}0$ ms, was similar to that observed in the rising phase of the twitch at this sarcomere length.

Sarcomere length dependence

The magnitude of the birefringence change associated with tetanic stimulation is reduced as the sarcomere length is increased beyond 2·6 μm (Fig. 6). The dependence of the birefringence change on sarcomere length is roughly similar to that of tension. Both signals show an initial rapid change soon after the start of stimulation followed by a roughly linear 'creep' phase that is more prominent at greater sarcomere length. Tension creep is due to slow development of increased sarcomere length dispersion along the fibres (see Fig. 10). In the central region of the fibres, where the optical recordings were made, sarcomeres are usually stretched during the creep phase, and this may be responsible for the downward creep in birefringence. Preliminary experiments showed a birefringence decrease associated with ramp stretch of active fibres (data not shown), which supports this interpretation of the birefringence changes during creep.

Retardation was measured after 0·4 s of tetanic stimulation, when the initial rising phase was complete but before substantial creep had taken place. Birefringence values were calculated from the optical path length obtained from photographs taken at the same time in the tetanus, and are plotted against sarcomere length (also measured from these photographs) in Fig. 7. The line through the data points was obtained by linear regression and intersects the sarcomere length axis at $3{\cdot}65 \pm 0{\cdot}08$ μm.

These results suggest that, within the precision of these measurements, the

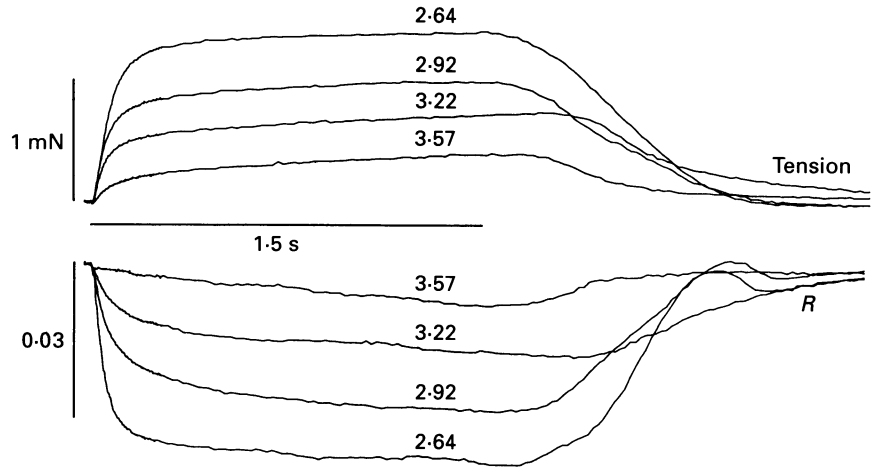

Fig. 6. Changes in tension (top) and intensity ratio R (bottom) associated with 1·5 s tetani at resting sarcomere lengths 2·64, 2·92, 3·22 and 3·57 μm, as indicated. Slit widths were 170, 168, 157 and 148 μm, and compensator retardations (θ) were 0·612, 0·547, 0·535 and 0·509 rad respectively. Before stimulation fibre widths were 107, 101, 98 and 76 μm respectively; depths, 61, 56, 57, 56 μm; peak retardations at thickest part of fibre cross-section (ϕ_c), 1·21, 1·28, 1·16, 1·32 rad; $(I_0+I_{90})/I_i$, 0·960, 0·967, 0·964, 0·958. At 0·4 s after the first stimulus sarcomere lengths were 2·60, 2·94, 3·24, 3·59 μm; widths, 108, 102, 98, 74 μm; depths, 62, 55, 55, 56 μm; $(I_0+I_{90})/I_i$, 0·963, 0·966, 0·966, 0·960. Sample interval was 2 ms for the first 150 ms and 20 ms thereafter. The horizontal bar marks the stimulus.

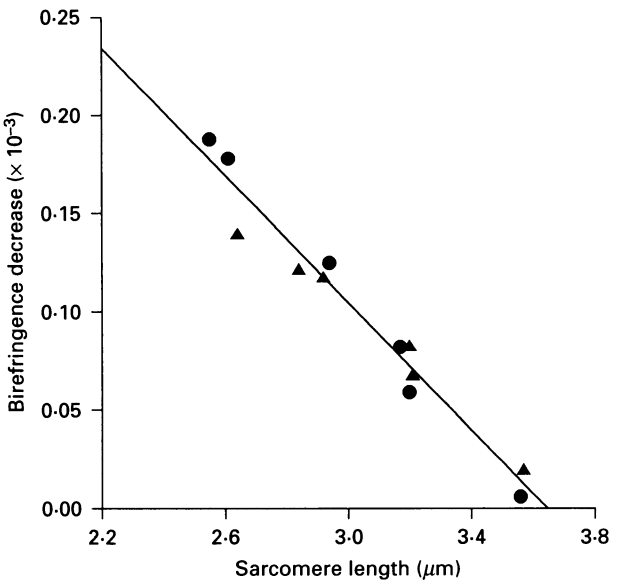

Fig. 7. Dependence of the magnitude of the birefringence decrease measured at 0·4 s after the start of tetanic stimulation on sarcomere length, from the experiment in Fig. 6 (▲) and a similar experiment in another fibre (●). Birefringence changes were calculated from observed values of R, $(I_0+I_{90})I_i$, compensator retardation, fibre depth and fibre width as described in the text. Sarcomere length was measured from photographs taken at 0·4 s in the tetanus. The straight line through the data was obtained by linear regression; it has slope $-0{\cdot}162\times10^{-3}$ μm^{-1} and birefringence intercept $0{\cdot}591\times10^{-3}$.

birefringence change associated with tetanic stimulation is proportional to the degree of overlap between myosin- and actin-containing filaments. At full filament overlap (sarcomere length 2·2 μm) the birefringence change predicted from the data in Fig. 7 is $0{\cdot}235 \pm 0{\cdot}015 \times 10^{-3}$.

Fig. 8. Changes in tension (top), fibre length (centre) and intensity ratio R (bottom) associated with a 1·5 s tetanus at resting sarcomere length 2·55 μm; fibre slightly compressed between glass plates. A release of 0·92 % fibre length, complete in 0·2 ms, was imposed at 1 s in the tetanus. Peak retardation at the thickest part of fibre cross-section (ϕ_c) before compression, 2·85 rad; after compression, 2·59 rad. The compensator retardation (θ) was set to the latter value before the start of the trace. Fibre length at 2·55 μm sarcomere length, 7·3 mm; width, 143 μm; depth, not measured. Sample interval was 1 ms for the first 550 ms and 10 ms thereafter. The latter is inadequate to resolve the changes associated with the length step; these are shown with a faster sampling rate in Fig. 9. The horizontal bar marks the stimulus.

Retardation measurements in fibres compressed between glass coverslips

The principal results obtained by the wide-field illumination method (Figs 4–6) were checked by an independent approach. Fibres were slightly compressed between parallel glass coverslips (see Methods) and the incident light beam was confined to a region of uniform path length in the centre of the fibre cross-section. Thus each part of the light beam experiences the same retardation (ϕ) on passing through the fibre, and the measured photodiode intensity ratio (R) is simply given by:

$$R = (I_0 - I_{90})/(I_0 + I_{90}) = \sin(\phi - \theta),$$

where θ is the retardation introduced by the compensator (eqn (A10)).

The optical path length could not be measured in compressed fibres, so absolute values of birefringence could not be obtained. However, since the optical path length remains constant on activation of the fibres, the fractional change in birefringence is equal to the observed fractional change in ϕ. As the degree of fibre compression was

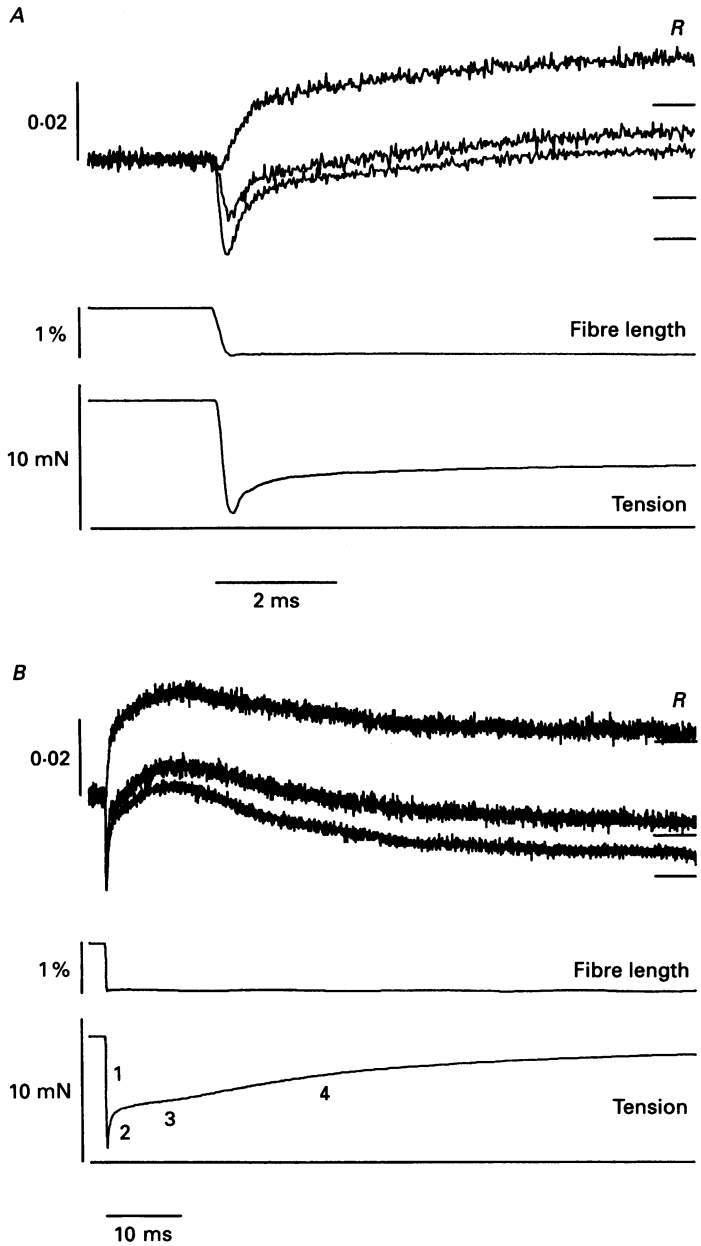

Fig. 9. Changes in intensity ratio R (top three traces), fibre length (centre) and tension (bottom) associated with a shortening step of 0·92% fibre length, complete in 0·2 ms, imposed during the plateau of a tetanus. A and B show parts of the same traces on fast (A) and slow (B) time scales. The four phases of the tension transient are labelled in B. Same fibre as Fig. 8; fibre slightly compressed between glass plates; resting sarcomere length 2·55 μm. The three R traces were obtained at three different sites along the fibre; peak retardation at the thickest part of fibre cross-section (ϕ_c) was 2·87, 2·64 and 2·52 rad at the three sites (reading downwards from the upper trace shown). The compensator retardation (θ) was set to these values during the tetani. The short horizontal lines at the

increased both the resting retardation and the amplitude of the retardation change associated with stimulation decreased, but the fractional change in retardation on activation was constant over a range of compression of about 30 μm. The isometric tension response was also unaffected by this degree of compression.

Figure 8 shows the R signal during a 1·5 s tetanus at initial sarcomere length 2·6 μm, in which a small shortening step was imposed on a compressed fibre. (The birefringence changes associated with shortening steps are considered in detail below.) The retardation changes associated with the isometric parts of the tetanus are similar to those recorded by the wide-field method (compare Fig. 8 with Fig. 6). The mean retardation decrease at 0·4 s in a tetanus was $8{\cdot}11 \pm 1{\cdot}05$% of the resting value (S.E.M., three fibres). Assuming a resting birefringence of $2{\cdot}20 \times 10^{-3}$ (Fig. 2) this corresponds to a birefringence decrease of $0{\cdot}178 \pm 0{\cdot}023 \times 10^{-3}$, similar to the value measured by the wide-field method ($0{\cdot}156 \pm 0{\cdot}018 \times 10^{-3}$). Pooling the data from the two methods gives a mean decrease of $0{\cdot}167 \pm 0{\cdot}012 \times 10^{-3}$ (S.E.M., six fibres). The time to half-maximum retardation, and hence birefringence, during the rising phase of the tetanus in the slightly compressed fibres was $48{\cdot}8 \pm 6{\cdot}9$ ms, and the time to half-maximum tension was $60{\cdot}0 \pm 5{\cdot}9$ ms. The paired difference, $11{\cdot}2 \pm 2{\cdot}1$ ms, is also similar to that found by the wide-field method, $11{\cdot}7 \pm 2{\cdot}0$ ms. The pooled mean is $11{\cdot}5 \pm 1{\cdot}3$ ms ($n = 6$). The peak birefringence change in a twitch in compressed fibres was $0{\cdot}140 \pm 0{\cdot}033 \times 10^{-3}$, compared with $0{\cdot}160 \pm 0{\cdot}017 \times 10^{-3}$ in the wide-field method; the pooled mean is $0{\cdot}150 \pm 0{\cdot}017 \times 10^{-3}$ ($n = 6$).

The fibre compression method did not completely remove movement artifacts in the R signals during the later part of mechanical relaxation. The extensive longitudinal movements of the central part of the fibre in this period may bring regions of slightly different birefringence into the illuminated region. Recovery of the R signal in the early part of relaxation was consistently slower than that of tension, however (Fig. 8).

Rapid shortening steps

Small shortening steps lasting 0·2 ms were applied during the plateau of isometric tetani in order to characterize the retardation changes associated with the transient tension response to such steps. The tension response to a shortening step of about 1% fibre length in slightly compressed fibres (Fig. 9) showed the characteristic four phases (A. F. Huxley & Simmons, 1971). Tension fell during the length step (phase 1), then showed a rapid partial recovery over the next few milliseconds (phase 2). The rate of tension recovery reached a minimum about 10 ms after the step (phase 3) before tension finally recovered to the isometric level (phase 4). The tension transients were not affected by slight compression of the fibres between glass plates, but compression by more than about 20 μm led to truncation of the tension change in phases 1 and 2.

The retardation changes in response to such length steps are much smaller than those during the rising phase of the tetanus (Fig. 8) but, despite their small

---

right side of the R traces show the values reached 0·5 s after the length step. The long horizontal lines under the tension traces are the tension baselines. Sample interval was 20 μs.

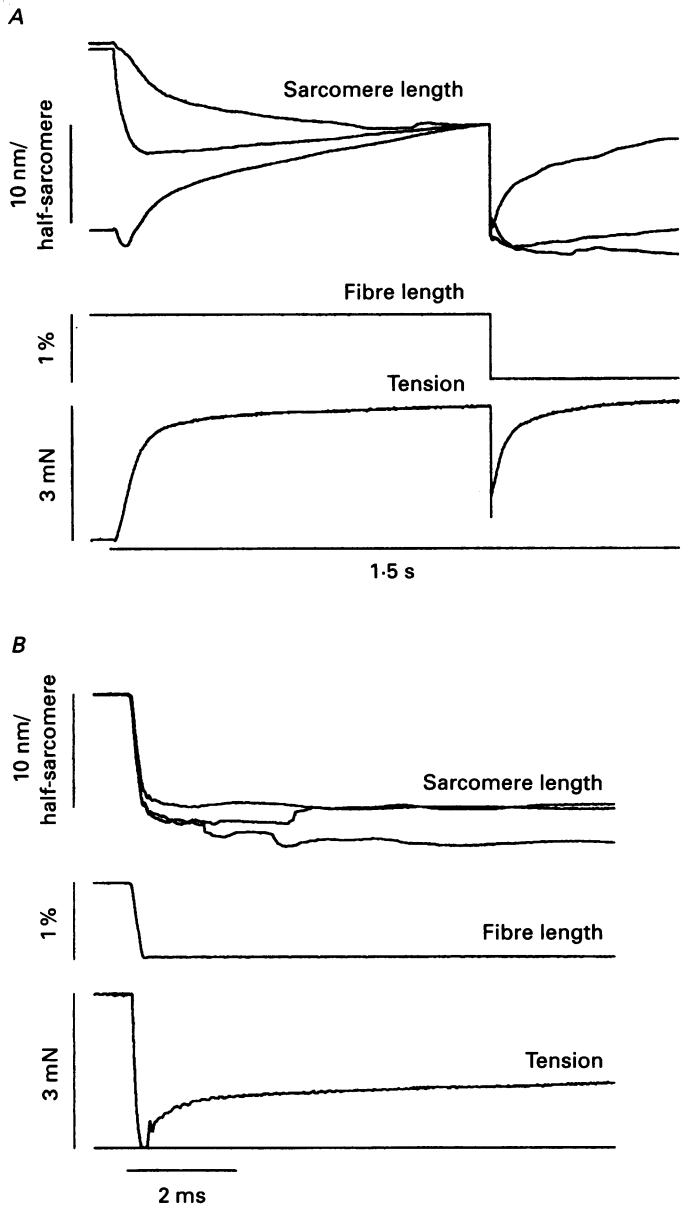

Fig. 10. Changes in mean sarcomere length (top three traces), fibre length (centre) and tension (bottom, with tension baseline shown in *B*) associated with a shortening step of 0·97 % (of fibre length at 2·2 μm), complete in 0·2 ms, imposed during the plateau of a tetanus. The top three traces were obtained from three different segments of the fibre, each of length 2·07 mm. The centres of the segments were 1·51, 4·89 and 3·68 mm (reading from the top) from the end of the fibre connected to the force transducer. The sarcomere length traces have been moved vertically to align at the start of the length step. Resting mean sarcomere lengths in the three segments were 2·61, 2·60 and 2·63 μm. Fibre length at 2·2 μm was 5·87 mm, cross-sectional area was 16020 μm^2. The horizontal bar in *A* marks the stimulus. Sample rates were 1 ms in *A* and 20 μs in *B*.

amplitude, components corresponding to the four phases of the tension response could readily be distinguished. Figure 9 shows retardation transients on two different time scales recorded from three sites along one fibre. The phase 1 retardation response was variable in both amplitude and direction; the mean change in three fibres (taking the average response from about six sites per fibre) was $-0{\cdot}08 \pm 0{\cdot}39\%$ of resting retardation (mean $\pm$ S.E.M., $n = 3$). The variability of the phase 1 response is likely to be due to movement artifacts during the length step which have not been eliminated by fibre compression.

During phase 2 of the tension response to a shortening step, which is considered to be associated with the elementary force-generating process in the actin-attached cross-bridge (A. F. Huxley & Simmons, 1971; Irving *et al.* 1992), the retardation showed a consistent increase (Fig. 9*A*). The mean amplitude of the increase, measured from the end of the length step to 2 ms later, was $0{\cdot}63 \pm 0{\cdot}05\%$ of the resting retardation, corresponding to a birefringence change of $0{\cdot}014 \pm 0{\cdot}001 \times 10^{-3}$. Retardation continued to increase during phase 3, reaching a peak value of $0{\cdot}91 \pm 0{\cdot}07\%$ resting retardation about 10 ms after the step (Fig. 9*B*).

Subsequently, in phase 4 of the tension transient, the retardation slowly recovered with a time course similar to that of the tension recovery. The mean retardation 0·5 s after the length step was $0{\cdot}36 \pm 0{\cdot}16\%$ less than that before the length step. There was a correlation between the retardation values 0·5 s after the length step (shown as short lines at the right-hand end of the traces in Fig. 9) and the corresponding values at the end of phase 1, consistent with the idea that the variable retardation change associated with phase 1 is due to a movement artifact which is mainly confined to the period of the length step.

Qualitatively similar R signals were obtained with the wide-field illumination method in uncompressed fibres. There was little change in R during a rapid shortening step, an increase corresponding to about 1% of the resting retardation during phase 2 of the tension transient, a further increase of about the same amplitude during phase 3, and recovery during phase 4.

The sarcomere length changes associated with shortening steps were measured in separate experiments with a striation follower (A. F. Huxley *et al.* 1981). Because of the technical limitations imposed by the striation follower, retardation was not measured in these experiments and the fibres were not compressed. All other experimental details, including stimulus timing, initial sarcomere length, amplitude and speed of length step were as in Figs 8 and 9. Since neither the retardation nor tension transients were affected by fibre compression, these dynamic sarcomere length measurements can be assumed to apply to the conditions of Figs 8 and 9. The sarcomere length changes during the fixed-end period of a tetanus in these conditions can vary substantially along a fibre; an extreme case in three segments of a single fibre is shown in Fig. 10*A* (top). In another fibre all the segments studied behaved like the central trace in the set of three in Fig. 10*A*, shortening during the initial tetanus rise, then slowly elongating.

In contrast with those during the first 1·5 s of a fixed-end tetanus, the sarcomere length changes associated with the early parts of the response to a shortening step were broadly similar in all segments studied (Fig. 10*B*). Most of the sarcomere shortening occurred during the applied length step, but there was a small additional

shortening during the rapid tension recovery (phase 2). The mean sarcomere shortening in these three segments, measured 2 ms after the end of the length step for comparison with the birefringence measurements, was 11·0 nm/half-sarcomere. In one of the segments the mean sarcomere length change was measured for shortening steps given at either 0·4 or 1·0 s in a tetanus from a resting sarcomere length of either 2·22 or 2·61 μm. There was no significant effect of varying either parameter (9·8 nm/half-sarcomere, 0·4 s, 2·22 μm; 9·7 nm/half-sarcomere, 1·0 s, 2·22 μm; 10·0 nm/half-sarcomere, 0·4 s, 2·61 μm; 9·6 nm/half-sarcomere, 1·0 s, 2·61 μm), confirming the absence of an effect of sarcomere creep on the sarcomere length change associated with shortening steps in the conditions used here. Similar results were obtained in another fibre. Mean sarcomere length changes 2 ms after the end of a shortening step in three segments were 9·2, 9·8 and 9·2 nm/half-sarcomere when the release was given at 1 s in a tetanus at resting sarcomere length 2·55 μm; the corresponding value for the first segment was 8·7 nm/half sarcomere when the release was given at 0·4 s from resting sarcomere length 2·16 μm.

DISCUSSION

Measurement of muscle birefringence changes

Birefringence is obtained from the ratio of two quantities: the optical retardation (the phase lag between two polarized light components leaving the muscle fibre) and the optical path length in the fibre. The retardation can be measured accurately, with negligible error due to fibre absorbance, reflectance or scattering (see Appendix). Measuring the path length in the fibre is more difficult, particularly in active contractions. Two approaches to this problem were used here.

In the wide-field illumination method (Figs 3–7) the light beam was wider than the fibre. Optical path length was measured by rotating the fibre about its axis by 90 deg and measuring its apparent diameter from photographs taken at rest or during contraction. Birefringence was calculated assuming that the cross-sectional shape of the fibres is elliptical. The error in this method was estimated as about 1% of the resting birefringence (see Appendix), which is an order of magnitude smaller than the change associated with isometric contraction. Consistent with this, little fibre-to-fibre variability was observed in the amplitude or time course of the retardation signals during the rising phase of the contraction.

An independent set of retardation measurements was made on fibres lightly compressed between glass plates (Figs 8 and 9). Optical path length is constant in the compressed region of the fibre, and errors due to changes in fibre cross-section should be removed. The compression itself might have introduced artifacts, for example by altering the normal fibre structure, but such artifacts appear to be small. The fractional change in retardation associated with contraction was independent of the degree of compression in the range used, and the amplitude and time course of the retardation changes during the rising phase of the contractions were similar in different fibres. The mean values of these parameters agreed with those obtained by the wide-field method. Both methods showed movement artifacts during the later part of relaxation (Figs 6 and 8). These may be due to real changes in birefringence at the optical recording site produced by longitudinal movements of a fibre which has small variations of birefringence along its length.

The birefringence changes associated with rapid shortening steps are difficult to measure accurately because they are much smaller than those accompanying the rising phase of activation (Fig. 8). Fortunately, the accompanying fibre shape changes are also much smaller. Retardation transients in response to shortening steps were qualitatively similar with the wide-field and compressed fibre methods, but the former were not used for quantitative measurements because path length could not be measured with sufficient accuracy. In compressed fibres the retardation transients associated with shortening steps of about 1% fibre length were reproducible after the end of the shortening step but variable during the step itself (Fig. 9). Movement artifacts of variable sign and typical amplitude 0·5% of resting retardation occurred during the length step. These could be related to longitudinal movements of the fibre, as in the case of the later part of mechanical relaxation.

Comparison with previous results

The resting birefringence was measured as $2{\cdot}20 \pm 0{\cdot}02 \times 10^{-3}$ at sarcomere length 2·4–2·7 μm and $2{\cdot}35 \pm 0{\cdot}03 \times 10^{-3}$ at sarcomere length 3·5–3·8 μm. These values are similar to the value of $2{\cdot}25 \times 10^{-3}$ measured by Baylor & Oetliker (1977) for frog fibres at 1·3 times slack length (sarcomere length probably about 2·7 μm). Values in the older literature are variable but their average is $2{\cdot}2 \times 10^{-3}$ (Høncke, 1947, p. 144).

The birefringence decrease associated with isometric contraction is similar to that reported for isolated frog fibres by Eberstein & Rosenfalck (1963), who found a decrease of about 9% at the peak of a twitch or tetanus at sarcomere length 2·2 μm, 7 °C. Using a resting birefringence of $2{\cdot}20 \times 10^{-3}$, this corresponds to a decrease of $0{\cdot}20 \times 10^{-3}$, similar to the value $0{\cdot}235 \pm 0{\cdot}015 \times 10^{-3}$ reported here. A decrease of similar size, $0{\cdot}265 \pm 0{\cdot}216 \times 10^{-3}$ (mean ± S.D., $n = 62$), in isometric tetani in isolated frog fibres has also been reported in the first-order diffracted beam (Burton, Baskin & Yeh, 1990). Eberstein & Rosenfalck found that the peak birefringence change in twitches at 7 °C decreased with increasing sarcomere length in the range 2·2–3·8 μm; its value at sarcomere length 3·6 μm was about 10% of that at 2·2 μm (cf. Fig. 7). They also found that the time to half-maximum birefringence change was less than that to half-maximum tension in a twitch, by an average of 13·5 ms at sarcomere length 2·4 μm, 7 °C and 6·0 ms at 12 °C, again in approximate agreement with the value reported above, $8{\cdot}8 \pm 1{\cdot}0$ ms at sarcomere length 2·6 μm, 3 °C. Eberstein & Rosenfalck did not measure optical path length during contraction or immobilize the fibres. However, they did reject fibres which showed more than a 1% change in light transmission in non-polarized wide-field illumination, and this may have effectively selected against those fibres in which there was a large change in cross-sectional shape on activation. Their results are clearly different from those of earlier work on whole muscles, which showed larger birefringence decreases with a complex time course (von Muralt, 1932; Bozler & Cottrell, 1937).

Origin of the birefringence changes

Muscle birefringence is caused by the alignment of contractile filaments with the fibre axis. In principle, the decrease in birefringence during contraction could be due to a decrease in either the fractional volume of the oriented proteins or in their degree of alignment. Small decreases in fractional volume produce proportional decreases in birefringence (Fredericq & Houssier, 1973; Peckham & Irving, 1989), so an increase

in fibre volume of about 7% would be required to produce the 7% birefringence decrease in isometric contraction at sarcomere length 2·6 μm. The actual volume change in these conditions was estimated to be less than 1% from the apparent diameter of the fibre along two perpendicular axes and the sarcomere length, assuming that the cross-sectional shape of the fibre does not change during contraction. This approximately isovolumetric behaviour is consistent with X-ray diffraction studies of isolated frog fibres under similar conditions (Cecchi, Griffiths, Bagni, Ashley & Maeda, 1991).

In the absence of sufficiently large volume changes, the birefringence signals must be due to changes in protein orientation. Muscle birefringence is dominated by the contribution of the myosin-containing A (anisotropic) bands of the sarcomere, so myosin is the most likely candidate for the orientation change. The myosin filaments themselves do not change orientation substantially during contraction, but the myosin cross-bridges undergo large movements (H. E. Huxley & Brown, 1967; H. E. Huxley, Faruqi, Kress, Bordas & Koch, 1982). Changes in the orientation of myosin cross-bridges are likely to be responsible for the birefringence changes during contraction.

This hypothesis is supported by the present results. The birefringence change is proportional to the degree of overlap between actin and myosin filaments, i.e. to the fraction of cross-bridges which can bind to actin (Fig. 7). The birefringence change precedes tension development in the rising phase of a tetanus, by $11{\cdot}5 \pm 1{\cdot}3$ ms at half-maximum. This temporal lead is similar to that of stiffness under comparable conditions, 11–16 ms (Ford, Huxley & Simmons, 1986; Cecchi *et al.* 1991; Irving, Månsson, Simmons, Piazzesi, Lombardi, Ferenczi & Harries, 1991). The lead of birefringence over tension could not be explained by series compliance, which is small in this preparation and has little effect on the lag between stiffness and tension (Irving *et al.* 1991). The time course of the birefringence change is also similar to that of the changes in intensities of the inner equatorial X-ray reflections, which are sensitive to the transfer of mass from near the myosin filaments to near the actin filaments as cross-bridges bind to actin and lead tension by 10–20 ms in these conditions (Cecchi *et al.* 1991; Irving *et al.* 1991). Both stiffness and the equatorial intensities lag tension during the early part of relaxation (Cecchi *et al.* 1991), as does birefringence (Fig. 5). The time course of the birefringence change during isometric contraction is therefore consistent with that expected from a change in orientation of the cross-bridge as it binds to actin. This orientation change precedes the tension-generating transition in the attached cross-bridge.

The birefringence decrease during contraction therefore suggests that cross-bridges bind to actin with their long axis more perpendicular to the fibre axis than in resting muscle. This is consistent with the changes in the intensities of axial X-ray reflections during the rising phase of a tetanus (H. E. Huxley *et al.* 1982), the axial elongation of the diffuse X-ray scattering (Lowy & Poulsen, 1990), and electron micrographs of fibres rapidly frozen during contraction (H. E. Huxley, Popp, Ouyang & Sosa, 1992; Lenart, Franzini-Armstrong & Goldman, 1992).

The magnitude of the orientation change can be estimated from the birefringence using a simple model for the structure of the cross-bridge (Irving *et al.* 1988; Haskell *et al.* 1989; Peckham & Irving, 1989). The mean birefringence decrease associated

with contraction at full filament overlap, $0{\cdot}235 \pm 0{\cdot}015 \times 10^{-3}$, is similar to that produced by putting skinned frog fibres into rigor at the same sarcomere length, $0{\cdot}22 \pm 0{\cdot}01 \times 10^{-3}$ (Peckham & Irving, 1989). Both sets of results suggest a large rotation of the myosin head, or S-1 domain, with respect to the filament axis. The birefringence of the relaxed skinned fibres, $2{\cdot}29 \pm 0{\cdot}04 \times 10^{-3}$, is close to that of resting intact fibres, $2{\cdot}20 \pm 0{\cdot}02 \times 10^{-3}$ at the same lattice volume (Peckham & Irving, 1989), suggesting that the myosin head orientation is also similar. In the simplest case in which all of the myosin heads have the same orientation, the long axis of the head would be at about 30 deg to the filament axis in resting muscle and at about 50 deg in either rigor (Peckham & Irving, 1989) or contracting muscle. However, the birefringence of contracting muscle would also be consistent with the presence of a wide range of head orientations: for example, a population of detached heads with a preferred orientation more parallel to the fibre axis, and an attached fraction with a perpendicular orientation preference.

Rapid shortening steps

When a small, rapid shortening step is applied to an actively contracting muscle fibre, the tension decreases during the step (phase 1), then partially recovers over the next few milliseconds (phase 2) (A. F. Huxley & Simmons, 1971; Fig. 9*A*). The tension decrease reflects the elastic properties of the attached cross-bridge, and the rapid tension recovery is considered by many investigators to be due to the working stroke in the attached cross-bridge (A. F. Huxley & Simmons, 1971; Irving *et al.* 1992). A rapid shortening step of about 1% fibre length produced no consistent change in birefringence during the length step itself, but there was an increase of $0{\cdot}63 \pm 0{\cdot}05$% of the resting value during the rapid tension recovery (phase 2, Fig. 9*A*). Thus shortening of the elastic element in the cross-bridge does not produce a detectable change in myosin head orientation, but the working stroke does involve an orientation change, with the average axial angle becoming more parallel to the filament axis. This is consistent with the observation that the intensity of the 14·5 nm axial X-ray reflection does not change during a shortening step of about 0·5% fibre length, but decreases markedly during the subsequent rapid force recovery (Irving *et al.* 1992). The change in the intensity of the 14·5 nm X-ray reflection during the working stroke could have been produced by either myosin head rotation or relative axial translations between heads; the birefringence results now show that axial rotation of all or part of the head is likely to be involved.

The birefringence continues to increase slightly during phase 3 of the tension transient, when tension recovery slows down (Fig. 9*B*) and the intensity of the 14·5 nm X-ray reflection partially recovers (H. E. Huxley, Simmons, Faruqi, Kress, Bordas & Koch, 1983; Irving *et al.* 1992). Phase 3 is likely to involve cross-bridge detachment from actin (A. F. Huxley & Simmons, 1971) followed by reattachment in a state capable of executing another working stroke (Lombardi, Piazzesi & Linari, 1992), so the continued small increase in birefringence during phase 3 is rather unexpected. One possible explanation is that birefringence is more sensitive to cross-bridge detachment than is the intensity of the 14·5 nm X-ray reflection (which is high in resting as well as in isometrically contracting muscle), so the net increase of birefringence during phase 3 might be caused by a small fraction of detached cross-

bridges taking up a more axial orientation, as they do in resting muscle. During phase 4 of the tension transient the birefringence returns slowly to close to its pre-step value, accompanied by complete recovery of tension (Fig. 9*B*) and the 14·5 nm X-ray signal (H. E. Huxley *et al.* 1983), as the original cross-bridge orientation distribution is regained.

The birefringence increase during the working stroke (Fig. 9) is an order of magnitude smaller than the decrease associated with the rising phase of a twitch or tetanus (Fig. 8), and could be due to a small fraction of the myosin heads, about 10% of the total, detaching from actin and taking up an orientation like that in resting muscle. Stiffness decreases by roughly this amount after such a shortening step (Lombardi *et al.* 1992), which would be consistent with this explanation. Alternatively the birefringence increase could be due to a change in orientation of the attached heads during the working stroke. If all the myosin heads had an axial angle of 50 deg before the length step, the birefringence change in the working stroke would correspond to a change in orientation of only about 1 deg, which is much smaller than expected for a working stroke of about 10 nm in the 20 nm myosin head. However, if, as argued above, there is a broad range of head orientations in the steady state of isometric contraction before the step, each head could rotate through a much bigger angle. Birefringence cannot distinguish between axial angles γ and 180 deg $-\gamma$, so unidirectional rotation of heads with a broad orientation distribution would bring some of them towards 90 deg and others away from 90 deg, with opposite effects on the birefringence. The net change in birefringence would then be small. The observed birefringence change would be consistent with an axial head rotation large enough to produce a working stroke of the order of 10 nm as long as the axial angles of the myosin heads in isometric contraction are distributed on both sides of 90 deg with an axial spread of about 30 deg or greater. A similar isometric orientation distribution was recently proposed to explain the change in intensity of the 14·5 nm X-ray reflection following a step release (Irving *et al.* 1992).

APPENDIX

This section derives equations relating the measured intensities of polarized light components to the intrinsic optical properties of a muscle fibre.

Principle of the method

The muscle fibre is illuminated by a beam of light travelling perpendicular to the fibre axis (Fig. 11). The incident light is considered in terms of components linearly polarized with electric vector parallel and perpendicular to the fibre axis; these are referred to as 0 deg and 90 deg components, respectively. The illuminating light passes through a linear polarizer with its transmission axis at 45 deg to the fibre axis (Fig. 11). Neglecting for the moment the effect of any other polarizing components, the light reaching the fibre can be considered as the sum of 0 deg and 90 deg components of equal intensity and phase. Within the fibre these components have respective refractive indices n_0 and n_{90} and wavelengths λ/n_0 and λ/n_{90}, where λ is the wavelength *in vacuo*. The birefringence of the fibre (B) is defined as $n_0 - n_{90}$, and is positive. Initially it is assumed that the illuminated part of the fibre is sufficiently

small that all the light has the same path length (L) in the fibre. This path length corresponds to Ln_0/λ and Ln_{90}/λ wavelengths for the 0 deg and 90 deg components, respectively. On leaving the fibre the phase difference between these components, the optical retardation (ϕ), is $L(n_0-n_{90})/\lambda$ wavelengths, or, in radians:

$$\phi = 2\pi LB/\lambda. \tag{A1}$$

The aim of the present experiments was to determine B from measurements of ϕ and L. The latter was either measured directly or held constant so that fractional changes in B would be equal to those in ϕ. The rest of the Appendix explains the basis of the methods used to determine ϕ. The calculations use the Jones calculus (Shurcliff, 1962; Baylor *et al.* 1984). The electric vectors of the two orthogonal polarization components are represented as complex constants of the form $ae^{i\alpha}$, where a denotes amplitude, α phase and i is $\sqrt{(-1)}$. The components with electric vectors at 0 deg and 90 deg to the fibre axis are denoted by subscripts 0 and 90 and written as a column vector. In the experimental arrangement in Fig. 11 the fibre is illuminated with light of intensity I_i polarized at 45 deg to the fibre axis. The incident light is represented as:

$$\sqrt{(\tfrac{1}{2}I_i)}\begin{vmatrix}1\\1\end{vmatrix}.$$

The light leaving the fibre and collected by the objective can be written as:

$$\begin{vmatrix}E_0\\E_{90}\end{vmatrix} = \sqrt{(\tfrac{1}{2}I_i)}\begin{vmatrix}\sqrt{T_0}\,e^{-i\phi}\\\sqrt{T_{90}}\end{vmatrix}. \tag{A2}$$

T_0 and T_{90} are the transmittances of the 0 deg and 90 deg component intensities, respectively. These are less than unity because of absorbance, scattering and diffraction of light by the fibre. The measured values of T_0 and T_{90} depend on the apertures of the optical system as well as on intrinsic fibre properties. The optical retardation defined in eqn (A1) is represented by ϕ.

Steady-state measurement of optical retardation

When ϕ is constant it can be determined by viewing the collected light through a second polarizer, the analyser (Fig. 11), with its transmission axis at 90 deg to that of the first polarizer. For polarizer (45 deg) and analyser (-45 deg) transmission axes (from eqn (A2)):

$$\begin{vmatrix}E_{45}\\E_{-45}\end{vmatrix} = \tfrac{1}{2}\sqrt{I_i}\begin{vmatrix}\sqrt{T_0}\,e^{-i\phi}+\sqrt{T_{90}}\\\sqrt{T_0}\,e^{-i\phi}-\sqrt{T_{90}}\end{vmatrix}. \tag{A3}$$

The intensity transmitted by the analyser, I_{-45}, is given by:

$$I_{-45} = |E_{-45}|^2 = \tfrac{1}{4}I_i(T_0+T_{90}-2\sqrt{(T_0T_{90})}\cos\phi) \tag{A4}$$

(cf. Fredericq & Houssier, 1973, eqn. 3·46; Peckham & Irving, 1989).

If a calibrated retardation compensator is introduced with its slow (higher refractive index) axis at 90 deg to the muscle fibre axis (Fig. 11) eqn (A4) becomes:

$$I_{-45} = \tfrac{1}{4}I_i(T_0+T_{90}-2\sqrt{(T_0T_{90})}\cos(\phi-\theta)), \tag{A5}$$

where θ is the compensator retardation. If $T_0 = T_{90}$ the observed intensity is zero when $\theta = \phi$. In fact $T_0 - T_{90}$ is small (see Results) and in the general case I_{-45} takes its minimum value when $\theta = \phi$, so ϕ can be measured by adjusting the compensator to achieve the darkest appearance of the field (Peckham & Irving, 1989).

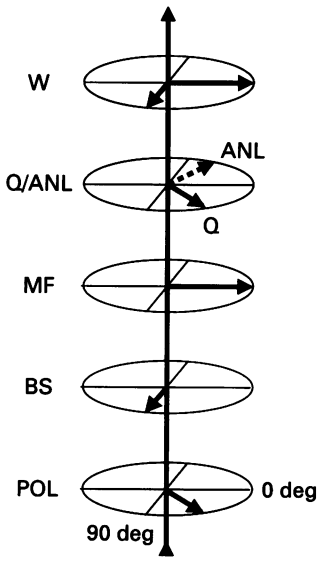

Fig. 11. Schematic diagram of the polarizing optical components used for fibre retardation measurements. POL, polarizer; BS, Babinet–Soleil compensator; MF, muscle fibre; Q, quarter-wave plate; ANL, analyser; W, Wollaston prism. The light is propagating vertically upwards. The horizontal axes labelled 0 deg and 90 deg denote directions parallel and perpendicular to the fibre axis, respectively. The arrows in the horizontal plane denote transmission axes for POL, ANL and W, and slow (larger retardation) axes for BS, MF and Q.

Continuous measurement of optical retardation

For continuous measurements of ϕ, the analyser (Fig. 11) was replaced by a quarter-wave plate with its slow axis at 45 deg to the fibre axis. The quarter-wave plate converts the phase difference introduced by the fibre into an intensity difference between 0 deg and 90 deg components. These two components can be separated by a Wollaston prism (Figs 1 and 11) and the intensities measured with photodiodes. The quarter-wave plate introduces an extra retardation of $\pi/2$ between the ± 45 deg components of the light collected by the objective. After transmission through the quarter-wave plate the amplitudes of the ± 45 deg components are given by:

$$\begin{vmatrix} E_{45} \\ E_{-45} \end{vmatrix} = \tfrac{1}{2}\sqrt{I_i} \begin{vmatrix} -i\sqrt{T_0}\,e^{-i\phi} - i\sqrt{T_{90}} \\ \sqrt{T_0}\,e^{-i\phi} - \sqrt{T_{90}} \end{vmatrix}. \tag{A6}$$

Resolving back to 0 deg, 90 deg axes and calculating intensities:

$$\begin{vmatrix} I_0 \\ I_{90} \end{vmatrix} = \tfrac{1}{4}I_i \begin{vmatrix} T_0 + T_{90} + 2\sqrt{(T_0\,T_{90})}\sin\phi \\ T_0 + T_{90} - 2\sqrt{(T_0\,T_{90})}\sin\phi \end{vmatrix}. \tag{A7}$$

The ratio $R = (I_0 - I_{90})/(I_0 + I_{90})$, which was calculated electronically, is given by:

$$R = 2\sqrt{(T_0 T_{90})} \sin\phi/(T_0 + T_{90}). \tag{A8}$$

If the quarter-wave plate is removed the corresponding intensity ratio is given by:

$$R_0 = (T_0 - T_{90})/(T_0 + T_{90}). \tag{A9}$$

In the case of a single muscle fibre, T_0 and T_{90} are almost equal, i.e. the polarization dependence of the total light scattering and absorbance, the dichroism, is very small (see below). Thus the use of the quarter-wave plate makes the retardation measurements very insensitive to dichroism, and for the purposes of the present measurements $T_0 = T_{90}$ and $R = \sin\phi$ (Taylor & Zeh, 1976). If a compensator is present, and introduces a retardation θ as in the previous section:

$$R = \sin(\phi - \theta). \tag{A10}$$

For small differences between fibre and compensator retardations, $\Delta R = \Delta(\phi - \theta)$, i.e. ΔR is numerically equal to the change in retardation (in radians) from the compensated value.

Wide-field illumination

The first series of retardation measurements (Figs 2–7) was made with an illuminating beam which was wider than the fibre, in order to minimize movement artifacts. In this case different regions of the light beam traverse different path lengths in the fibre, acquiring different retardations. However, the fibre birefringence can still be derived from the measured light intensities if the fibre is assumed to have an elliptical cross-section. Possible errors introduced by this assumption are considered below. The theoretical treatment for this case is analogous to that of A. F. Huxley in Eberstein & Rosenfalck (1963) and to that of Baylor *et al.* (1984).

The elliptical cross-section of the fibre has major and minor semi-axes a and b (Fig. 12). Initially the minor axis is assumed to be parallel to the direction of propagation of the light, the z-axis. The major axis is parallel to the y-axis and the fibre axis is parallel to x. The illuminating light is assumed to be a parallel beam of width s, corresponding to the image of the field slit at the fibre. The intensity contributions measured at the photodiodes from all the elements, dy, of the light beam are integrated across its width. Within the fibre the transmittance is assumed to be independent of the plane of polarization, i.e. $T_0 = T_{90} = T$. As in the uniform path length case (eqns (A8) and (A10)) this assumption gives a very good approximation to the measured intensity ratios from single muscle fibres (eqns (A15) and (A17) below).

For an element dy of slit which is not occupied by fibre, from eqn (A7):

$$\left|\begin{matrix} dI_0 \\ dI_{90} \end{matrix}\right| = I_i dy/2s \left|\begin{matrix} 1-\sin\theta \\ 1+\sin\theta \end{matrix}\right|. \tag{A11}$$

Similarly, for an element within the fibre:

$$\left|\begin{matrix} dI_0 \\ dI_{90} \end{matrix}\right| = TI_i dy/2s \left|\begin{matrix} 1+\sin\phi(y) \\ 1-\sin\phi(y) \end{matrix}\right|, \tag{A12}$$

where $\phi(y) = 2z.2\pi B/\lambda - \theta = \phi_c\sqrt{(1-y^2/a^2)} - \theta$, where ϕ_c is the retardation of the ray passing through the centre of the fibre, $\phi_c = 4\pi bB/\lambda$. Integrating across the slit width and assuming that T is independent of y, as shown in Results:

$$\begin{vmatrix} I_0 \\ I_{90} \end{vmatrix} = \tfrac{1}{2}I_i f \begin{vmatrix} 1-\sin\theta \\ 1+\sin\theta \end{vmatrix} + \tfrac{1}{2}I_i(1-f)T \begin{vmatrix} 1+S \\ 1-S \end{vmatrix}, \tag{A13}$$

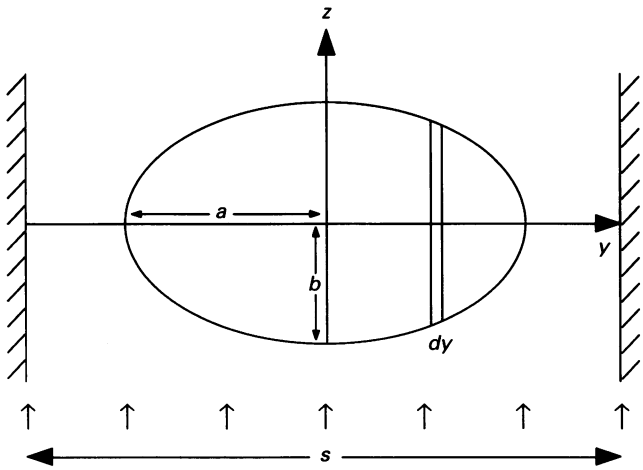

Fig. 12. Elliptical fibre cross-section assumed in retardation calculations for the case of wide-field illumination. The light is propagating along z, parallel to the minor axis of the fibre cross-section (semi-axis b). The fibre axis corresponds to the x-axis. The major axis of the fibre cross-section is along y (semi-axis a) and the image of the field slit at the fibre has width s.

where $f = 1-2a/s$ is the fraction of the light which bypasses the fibre and

$$S = \tfrac{1}{2}a\int_{-a}^{a} \sin[\phi_c\sqrt{(1-y^2/a^2)} - \theta]\,dy = \tfrac{1}{2}\pi J_1(\phi_c)\cos\theta - [1-\tfrac{1}{2}\pi.H_1(\phi_c)]\sin\theta, \tag{A14}$$

where J_1 and H_1 are, respectively, Bessel and Struve functions of first order. From eqn (A13):

$$R = (I_0 - I_{90})/(I_0 + I_{90}) = (1-g)S - g\sin\theta, \tag{A15}$$

and

$$(I_0 + I_{90})/I_i = f + (1-f)T = f/g, \tag{A16}$$

where $g = f/[(1-f)T+f]$ can be considered as the effective fraction of light passing the fibre, taking into account fibre transmittance. With the quarter-wave plate removed:

$$R_0 = (1-f)(T_0 - T_{90})/[2f + (1-f)(T_0 + T_{90})]. \tag{A17}$$

This relation was used to measure fibre dichroism $(T_0 - T_{90})$. The error in retardation measurements due to fibre dichroism (eqn (A9)) is extremely small; the effect is to multiply R values by a factor $2\sqrt{(T_0 T_{90})}/(T_0 + T_{90})$. With the mean values of $(T_0 - T_{90})$ and $(T_0 + T_{90})$ recorded with the present experimental set-up, this factor

has a value of 0·9999. The theoretical relation between R and θ (eqn (A15)) is compared with experimental data from relaxed fibres in Fig. 3 in the Results section, where it is shown that the theory gives a reasonable fit to the data.

Sensitivity of R to changes in fibre birefringence, transmittance and movement

Figure 13 shows the sensitivity of R to changes in fibre birefringence, transmittance and cross-sectional shape, calculated from eqns (A14) to (A16) for typical values of fibre parameters. R varies roughly linearly with fibre birefringence for small changes around the resting value (Fig. 13*A*). The time course of birefringence changes was estimated in the Results section by assuming that they were linearly related to changes in R. The degree of non-linearity in Fig. 13*A* would produce an error in the estimate of time to half-peak birefringence in a twitch or tetanus (Figs 4–6) of less than 1 ms. The sensitivity of R to changes in birefringence decreases with increasing ϕ_c and g in the range used in the present work. The method becomes unreliable (R is relatively insensitive to birefringence changes or the linearity is poor) when ϕ_c is greater than π, i.e. when the maximum optical path length in the fibre is greater than about 150 μm. For this reason measurements were made with the minor diameter of the fibre cross-section parallel to the light path; this diameter was always less than 130 μm. In this case the value of g had to be less than about 0·4 for adequate sensitivity, although g values of up to 0·5 were usable with small fibres.

There is a slight increase in R with increasing fibre transmittance T (Fig. 13*B*). Because the amplitude of birefringence changes was calculated from eqn (A15) using simultaneously measured values of T and R, errors in birefringence amplitudes due to transmittance changes are negligible. Figure 13*C* shows the effect on R of a change in the axial ratio of the elliptical cross-section from its initial value of 1·6, keeping fibre volume constant. The main effect is due to a change in the fraction of light going past the fibre. This type of error was avoided by measuring major and minor diameters of the fibre at rest and during contraction. R is also sensitive to rotation of the fibre about its long axis (Fig. 13*D*). The effect of rotation is equivalent to a decrease of axial ratio (see legend to Fig. 13) and, as in that case, errors in birefringence can be avoided by measuring fibre diameters along two perpendicular directions. R is relatively insensitive to rotations of less than 10 deg (Fig. 13*D*); the effect becomes significant when the rotation is large enough to change the fraction of the light bypassing the fibre.

The above calculations assume that the fibre cross-section is an ellipse, but this is not a good approximation for some fibres or fibre regions (Blinks, 1965). Deviations from elliptical cross-section are likely to produce the largest source of error in applying the theory developed in eqns (A11)–(A17) to real muscle fibres, and may be responsible for the imperfections in the fit of the theory to experimental data from resting fibres (Fig. 3*B*). Errors in birefringence *changes* due to a change in fibre shape are limited by the measurements of changes of apparent fibre diameter along two perpendicular axes. Only those fibres for which both apparent diameters changed by less than 3% were used for analysis of birefringence measurements with wide-field illumination (Figs 4–7) and this makes large changes in fibre shape unlikely. Some types of shape change would not be detected: for example, if the ellipse of Fig. 12 became a 160 μm section of a wedge, height 100 μm at one edge and 57 μm at the

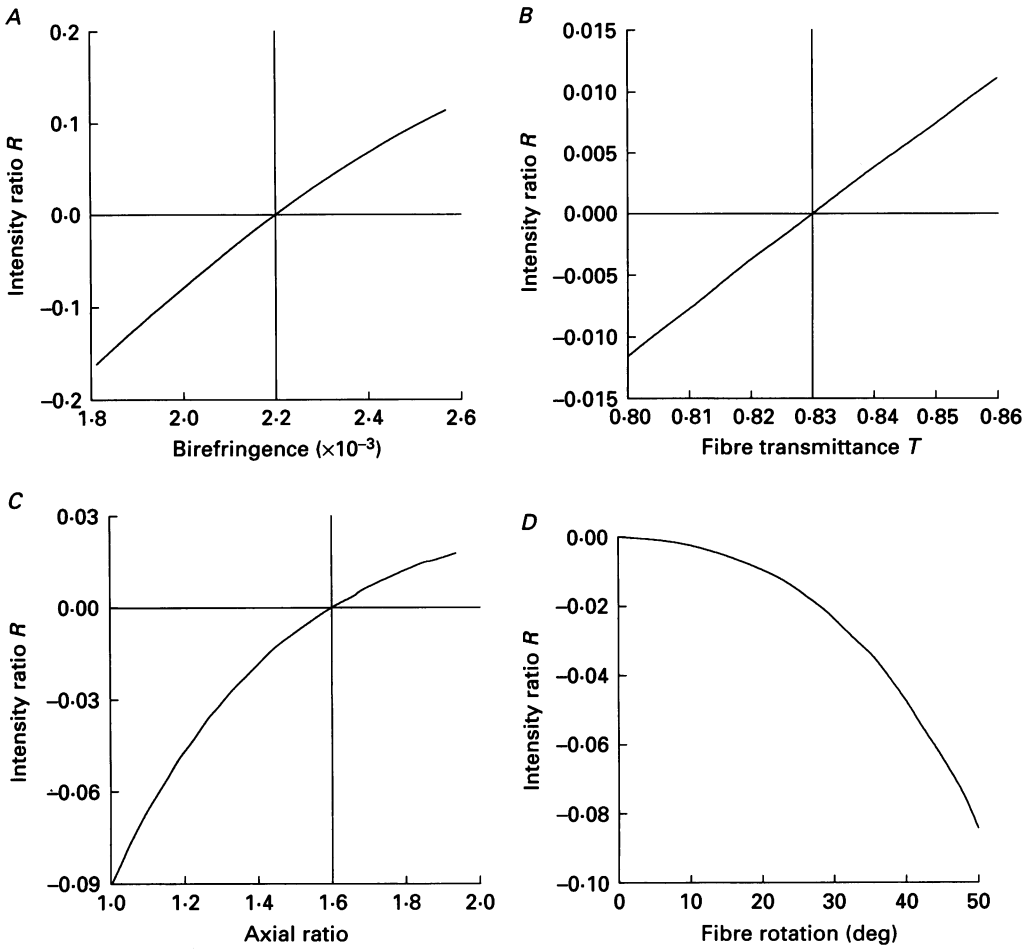

Fig. 13. Dependence of the intensity ratio R on birefringence (A), fibre transmittance (B), axial ratio of fibre cross-section (C) and rotation of the fibre cross-section (D), calculated from eqns (A14)–(A16) for typical values of fibre parameters. The cross-section of the fibre is initially an ellipse, major diameter 160 μm, minor diameter 100 μm, with the minor diameter parallel to the direction of light propagation. The resting birefringence is assumed to be $2{\cdot}20 \times 10^{-3}$ (Fig. 2) so ϕ_c, the retardation at the thickest part of the fibre cross-section, is 220 nm or 2·18 rad. Fibre transmittance T was taken to be 0·83, and the fraction of light passing the fibre, f, as 0·3, giving $g = 0{\cdot}341$. The compensator retardation, θ, was assigned the value required to give $R = 0$ ($\theta = 1{\cdot}17$ radians). These values are close to the means observed in the fibre experiments. When an ellipse with major and minor semi-axes a and b (and the minor axis initially parallel to the light beam) rotates through an angle β, it can be shown that the distribution of optical path lengths is the same as that of an ellipse with semi-axis $\sqrt{(a^2\cos^2\beta + b^2\sin^2\beta)}$ perpendicular to the light beam and $ab/\sqrt{(a^2\cos^2\beta + b^2\sin^2\beta)}$ parallel to the light beam. Thus rotation of the ellipse is equivalent to a decrease in axial ratio.

other, the area and apparent diameters would remain unchanged, but R would increase by 0·015. This extreme case corresponds to an apparent birefringence change of about 1·8% of the resting value.

I thank the Wellcome Trust, the Royal Society and the Medical Research Council (UK) for financial support and M. L. Clarke, Y. E. Goldman, A. F. Huxley, N. Millar, M. Peckham and R. M. Simmons for helpful comments on an earlier version of the manuscript. I am particularly grateful to R. M. Simmons for his generous help in initiating this project and to V. Lombardi and G. Piazzesi for help and discussion.

REFERENCES

BAYLOR, S. M., CHANDLER, W. K. & MARSHALL, M. W. (1984). Calcium release and sarcoplasmic reticulum membrane potential in frog skeletal muscle fibres. *Journal of Physiology* **348**, 209–238.

BAYLOR, S. M. & OETLIKER, H. (1977). The optical properties of birefringence signals from single muscle fibres. *Journal of Physiology* **264**, 163–198.

BLINKS, J. R. (1965). Influence of osmotic strength on cross-section and volume of isolated single muscle fibres. *Journal of Physiology* **17**, 42–57.

BOZLER, E. & COTTRELL, C. (1937). The birefringence of muscle and its variation during contraction. *Journal of Cellular and Comparative Physiology* **10**, 165–182.

BURTON, K., BASKIN, R. J. & YEH, Y. (1990). Crossbridge activity monitored from the state of polarisation of light diffracted by activated frog muscle fibres. *Journal of Muscle Research and Cell Motility* **11**, 258–270.

CECCHI, G., COLOMO, F. & LOMBARDI, V. (1976). A loudspeaker servo system for determination of mechanical characteristics of isolated muscle fibres. *Bollettino della Società italiana di biologia sperimentale* **52**, 733–736.

CECCHI, G., GRIFFITHS, P. J., BAGNI, M. A., ASHLEY, C. C. & MAEDA, Y. (1991). Time-resolved changes in equatorial X-ray diffraction and stiffness during rise of tetanic tension in intact length-clamped single muscle fibres. *Biophysical Journal* **59**, 1273–1283.

COOKE, R. (1986). The mechanism of muscle contraction. *CRC Critical Reviews in Biochemistry* **21**, 53–118.

EBERSTEIN, A. & ROSENFALCK, A. (1963). Birefringence of isolated muscle fibers in twitch and tetanus. *Acta Physiologica Scandinavica* **57**, 144–166.

FORD, L. E., HUXLEY, A. F. & SIMMONS, R. M. (1977). Tension responses to sudden length change in stimulated frog muscle fibres near slack length. *Journal of Physiology* **269**, 441–515.

FORD, L. E., HUXLEY, A. F. & SIMMONS, R. M. (1986). Tension transients during the rise of tetanic tension in frog muscle fibres. *Journal of Physiology* **372**, 595–609.

FREDERICQ, E. & HOUSSIER, C. (1973). *Electric Dichroism and Electric Birefringence*. Clarendon Press, Oxford.

HASKELL, R. C., CARLSON, F. D. & BLANK, P. S. (1989). Form birefringence of muscle. *Biophysical Journal* **56**, 401–413.

HØNCKE, P. (1947). Investigations on the structure and function of living, isolated, cross striated muscle fibres of mammals. *Acta Physiologica Scandinavica* **15**, suppl. 48.

HUXLEY, A. F. (1977). Looking back on muscle. In *The Pursuit of Nature*, ed. HODGKIN, A. L. Cambridge University Press, Cambridge, UK.

HUXLEY, A. F. & LOMBARDI, V. (1980). A sensitive force transducer with resonant frequency 50 kHz. *Journal of Physiology* **305**, 15–16*P*.

HUXLEY, A. F., LOMBARDI, V. & PEACHEY, L. D. (1981). A system for fast recording of longitudinal displacement of a striated muscle fibre. *Journal of Physiology* **317**, 12–13*P*.

HUXLEY, A. F. & SIMMONS, R. M. (1971). Proposed mechanism of force generation in striated muscle. *Nature* **233**, 533–538.

HUXLEY, H. E. & BROWN, W. (1967). The low-angle X-ray diagram of vertebrate striated muscle and its behaviour during contraction and rigor. *Journal of Molecular Biology* **30**, 383–434.

HUXLEY, H. E., FARUQI, A. R., KRESS, M., BORDAS, J. & KOCH, M. H. J. (1982). Time-resolved X-ray diffraction studies of the myosin layer-line reflections during muscle contraction. *Journal of Molecular Biology* **158**, 637–684.

HUXLEY, H. E., POPP, D., OUYANG, G. & SOSA, H. (1992). Crossbridges in frozen contracting muscle. *Biophysical Journal* **61**, A300.

HUXLEY, H. E., SIMMONS, R. M., FARUQI, A. R., KRESS, M., BORDAS, J. & KOCH, M. H. J. (1983). Changes in the X-ray reflections from contracting muscle during rapid mechanical transients and their structural implications. *Journal of Molecular Biology* **169**, 469–506.

IRVING, M. (1987). Muscle mechanics and probes of the crossbridge cycle. In *Fibrous Protein Structure*, ed. SQUIRE, J. M. & VIBERT, P. J., pp. 495–528. Academic Press, London.

IRVING, M., LOMBARDI, V., PIAZZESI, G. & FERENCZI, M. A. (1992). Myosin head movements are synchronous with the elementary force-generating process in muscle. *Nature* **357**, 156–158.

IRVING, M., MÅNSSON, A., SIMMONS, R. M., PIAZZESI, G., LOMBARDI, V., FERENCZI, M. A. & HARRIES, J. (1991). Equatorial X-ray diffraction, stiffness and force time courses during segment length-clamp of tetanized intact fibres isolated from *Rana temporaria* muscle. *Journal of Physiology* **438**, 147*P*.

IRVING, M., PECKHAM, M. & FERENCZI, M. A. (1988). Birefringence as a probe of cross-bridge orientation in demembranated muscle fibres. In *Molecular Mechanisms of Muscle Contraction*, ed. SUGI, H. & POLLACK, G. H., pp. 299–306. Plenum, New York.

LENART, T. D., FRANZINI-ARMSTRONG, C. & GOLDMAN, Y. E. (1992). Ultrastructure of frog sartorius muscle fibers quickly frozen following activation by caged Ca^{2+} photolysis. *Biophysical Journal* **61**, A286.

LOMBARDI, V., PIAZZESI, G. & LINARI, M. (1992). Rapid regeneration of the actin–myosin power stroke in contracting muscle. *Nature* **355**, 638–641.

LOWY, J. & POULSEN, F. R. (1990). Studies of the diffuse X-ray scattering from contracting frog skeletal muscles. *Biophysical Journal* **57**, 977–985.

MURALT, A. VON (1932). Über das verhalten der Doppelbrechung des quergestreiften muskels während der kontraktion. *Pflügers Archiv* **230**, 299–326.

NOLL, D. & WEBER, H. H. (1934). Polarisationoptik und molekularer Feinbau der Q-abschnitte des Froschmuskels. *Pflügers Archiv* **235**, 234–240.

OBIORAH, O. & IRVING, M. (1989). The intrinsic birefringence of skinned muscle fibres in aqueous and non-aqueous media. *Biophysical Journal* **55**, 462a.

PECKHAM, M. & IRVING, M. (1989). Myosin crossbridge orientation in demembranated muscle fibres studied by birefringence and X-ray diffraction measurements. *Journal of Molecular Biology* **210**, 113–126.

SHURCLIFF, W. A. (1962). *Polarised Light: Production and Use*. Harvard University Press, Cambridge, MA, USA.

TAYLOR, D. L. (1976). Quantitative studies on the polarisation optical properties of striated muscle. I. Birefringence changes of rabbit psoas muscle in the transition from rigor to relaxed state. *Journal of Cell Biology* **68**, 497–511.

TAYLOR, D. L. & ZEH, R. M. (1976). Methods for the measurement of polarisation optical properties. I. Birefringence. *Journal of Microscopy* **108**, 251–259.